

A Monte-Carlo model of xenon resonance radiation transport in a plasma display panel cell: Transition from optically thick to thin regimes

Trudy van der Straaten^{a)} and Mark J. Kushner^{b)}

Department of Electrical and Computer Engineering, University of Illinois, 1406 W. Green Street, Urbana, Illinois 61801

(Received 3 August 1999; accepted for publication 13 December 1999)

Plasma display panels (PDPs) are a promising technology for large-area flat panel color displays. The operation of PDPs relies on UV radiation from the $\text{Xe}(5p^56s \rightarrow 5s^25p^6)$ and $\text{Xe}(5p^56s' \rightarrow 5s^25p^6)$ resonance transitions, and the radiative relaxation of Xe_2^* , to excite phosphors, thereby producing visible radiation. The particular combination of device dimensions, gas composition, and operating conditions typically used in PDP cells is such that the resonance UV radiation is in a quasi-optically thick regime. In this article, results from a radiation transport model which accounts for the frequency redistribution resulting from multiple resonance absorption and re-emission is discussed. The model employs Monte-Carlo photon transport and frequency redistribution algorithms to treat the nonlocal nature of resonance radiation transport. Using results from this model, the transition from optically thin to optically thick transport is discussed for conditions typically used in conventional PDPs. © 2000 American Institute of Physics. [S0021-8979(00)05206-3]

I. INTRODUCTION

Plasma display panels (PDPs) are a promising technology for large-area high-brightness flat panel displays. The basic PDP cell consists of a noble gas mixture sealed between two dielectric sheets backed by electrodes. A transient discharge is initiated by applying a voltage pulse to the electrodes which leads to the emission of visible or UV light, depending on the gas mixture. Eventually charging of the dielectric surfaces shields the applied voltage and the discharge is quenched. By repeatedly pulsing the electrodes with voltages of alternating polarity, a continuous appearing light source can be maintained. Color PDP cells generally use xenon gas mixtures to generate UV photons that are converted to visible light through phosphors. A review of PDP technology can be found in Ref. 1.

To better characterize the operation of PDPs and to better understand the fundamental discharge physics of PDPs, several one- and two-dimensional models have been developed.²⁻¹² Most of these models have focused on the discharge dynamics. For example, Sahni and co-workers²⁻⁴ developed a one-dimensional (1D) fluid model to study the I - V characteristics of a monochrome neon-argon PDP, and found the dynamics to be sensitive to secondary electron emission from the dielectrics. Veerasingam *et al.* developed both 1D⁵ and two-dimensional (2D)⁶ fluid models, including a treatment of the external driving circuit, to investigate the temporal and spatial evolution of charged particle and excited state densities, and electrical characteristics of a helium-filled PDP cell. Using these models they were able to reproduce the qualitative behavior of measured I - V charac-

teristics. A 1D hybrid fluid model of a helium-filled PDP, incorporating a fully kinetic description of electron dynamics, was implemented by Drallos *et al.*⁷ Their results showed that, relative to kinetic simulations, the use of the local field approximation tends to overestimate ionization rates, particularly near the cathode, leading to lower predicted threshold voltages. Punset *et al.*⁸ developed a 2D, fluid model of adjacent PDP cells with opposing electrodes. They found that in the absence of barrier ribs the discharges in adjacent cells tend to overlap, making it difficult to separately control them.

Although models of PDPs have contributed significantly to our understanding of cell operation, less attention has been paid to UV photon transport. The UV radiation produced by resonance transitions of $\text{Xe}(5p^56s \rightarrow 5s^25p^6)$ and $\text{Xe}(5p^56s' \rightarrow 5s^25p^6)$ at wavelengths of 147 and 129 nm, respectively, are typically in a quasi-optically thick regime. That is, the mean free path for resonance reabsorption λ_a is smaller than typical cell dimensions resulting in radiation trapping. Radiation produced by the relaxation of the Xe_2^* excimer, which does not have a stable ground state, is not trapped so that the fraction of these photons that ultimately reaches the phosphor depends only on geometric factors.

Meunier *et al.*⁹ developed a 1D hybrid fluid PDP model which included a radiation transport model for UV emission resulting from the decay of both resonance atomic and excimer xenon states in a Ne/Xe=90/10 gas mixture at 560 Torr. Radiation trapping of the resonance Xe photons was accounted for by assuming an effective lifetime, calculated using a form of the Holstein theory of radiation transport.¹³ Emission from the 147 nm $\text{Xe}(5p^56s \rightarrow 5s^25p^6)$ resonance transition was found to be more intense than that of the excimer radiation. The authors concluded that radiation trapping is not efficient due to the small ($\approx 100 \mu\text{m}$) device

^{a)}Present address: Beckman Institute, MC 251, 405 N. Mathews, Urbana, IL 61801; electronic mail: trudyv@uiuc.edu

^{b)}Author to whom correspondence should be addressed; electronic mail: mjk@uiuc.edu

dimensions. Veerasingam *et al.*¹⁰ extended their 1D fluid code to describe UV radiation transport in a He/Xe gas mixture at 400 Torr, including a similar treatment of resonance photon trapping. For low Xe mole fractions ($\leq 10\%$) they found that the UV emission was dominated by the resonance decay of Xe($5p^56s$). However, as the Xe mole fraction was increased above $\approx 20\%$ radiation trapping was found to be important and the Xe₂^{*} excimer became the main source of UV radiation. Using a 2D hybrid fluid model with a Holstein treatment of radiation trapping, Rauf and Kushner^{11,12} found that for typical operating conditions (400 Torr and 200 V) and gas mixtures (Ne/He/Xe = 24/70/4), the UV flux to the phosphor is dominated by the nonresonance xenon dimer radiation. This model assumed that resonance radiation is in an optically thick regime.

In previous models, resonance photon trapping and transport were typically accounted for by multiplying the Einstein A coefficient for spontaneous decay by a trapping parameter, often called the Holstein factor, whose value is less than unity.¹³ The Holstein factor correctly describes the lengthening of the apparent lifetime of the resonance states due to radiation trapping. However, other than on a spatially averaged basis, it does not provide information on the location in the discharge from which the photons that do escape were emitted. Although most resonance photons are emitted with frequencies near line center and thus have a short mean free path for resonance reabsorption, the short radiative lifetime for spontaneous emission enables the photon to be re-emitted many times before being quenched or escaping from the plasma. Each time a photon is re-emitted it has a small but finite probability of being emitted from the wings of the line shape where the cross section for absorption is lower, thereby having a longer mean free path and higher probability for escaping the discharge. This process is typically called complete (or partial) frequency redistribution, an overview of which has recently been presented by Curry *et al.*¹⁴ and Lawler and Curry.¹⁵

In order to use the Holstein factor to determine the fraction of resonance radiation leaving the discharge an assumption must be made about the opacity of the radiation in all regions of the line shape and as a function of position. For example, Curry *et al.*¹⁴ found that the radiation trapping factor is a function of the radial distribution of the absorbing species in a cylindrical glow discharge. Both Meunier *et al.*⁹ and Veerasingam *et al.*¹⁰ in their PDP models assumed that all of the resonance radiation, though trapped, is optically thin since all photons emitted with the lengthened lifetime escaped from the plasma with the same probability. In contrast, Rauf and Kushner^{11,12} assumed that the resonance radiation is optically thick and so radiation incident on the phosphor is preferentially emitted from the edges of the discharge. These assumptions are accurate for resonance radiation transport in the two extremes of optically thick and optically thin regimes. The combination of operating pressures and discharge dimensions typically used in PDPs, though, is such that the resonance radiation may transition between being optically thin to optically thick.

To address radiation trapping in PDP cells, a radiation transport model has been developed which uses Monte-Carlo

(MC) photon transport and frequency redistribution algorithms.^{14,16} The Monte-Carlo frequency redistribution (MC-FR) model is described in Sec. II. Using this model, the spectra of resonance UV photons incident on the phosphor and their escape probabilities for varying concentrations of xenon in xenon–neon–helium gas mixtures were investigated and those results are presented in Sec. III. For typical operating conditions, the spectrum exhibits significant frequency redistribution due to absorption and subsequent re-emission. The escape probability is a strong function of the xenon concentration. Section IV contains concluding remarks.

II. DESCRIPTION OF THE MC-FR MODEL

The 2D PDP model used here is the same as that developed by Rauf and Kushner^{11,12} with the addition of the MC-FR radiation transport module. The PDP model contains a solution of the continuity and momentum transport equations for all charged and neutral species using a drift-diffusion formulation, Poisson's equation, and dielectric surface charging. Under typical PDP operating conditions the UV and visible light radiation do not noticeably affect the PDP discharge dynamics and, for the purpose of this study, were not directly coupled with the plasma hydrodynamics module. The MC-FR radiation transport model is a module invoked periodically during the PDP simulation to calculate the UV photon flux to all surfaces.

Each time the MC-FR module is invoked an ensemble of pseudophotons is initialized, representing the average density of photons emitted per second. The initial emission sites are distributed in space in proportion to the density of the radiating species. Emission is assumed to be isotropic and each pseudophoton is assigned an initial frequency chosen from the line shape function. Since, for the conditions of interest, both pressure and Doppler broadening are important, a Voigt line shape function $g(\bar{\nu})$ ¹⁷ is used

$$g(\bar{\nu}) = \frac{a}{\pi} \int_{-\infty}^{+\infty} \frac{e^{-y^2}}{a^2 + (\bar{\nu} - y)^2} dy, \quad (1)$$

where the integral is over all Xe atom velocities, $a = \Delta\nu_H / (4\pi\Delta\nu_D)$ is the ratio of the homogeneous linewidth $\Delta\nu_H$ to the Doppler width $\Delta\nu_D$, and $\bar{\nu} = (\nu - \nu_0) / \Delta\nu_D$ is the frequency departure from the line center ν_0 in units of the Doppler width. The Doppler width is given by

$$\Delta\nu_D = \left(\frac{8k_B T}{Mc^2} \right)^{1/2} \nu_0, \quad (2)$$

where M is the atomic mass of the radiating species, k_B is the Boltzmann constant, and T is the gas temperature. The homogeneous linewidth of a particular transition between states 1 and 2 is given by¹⁸

$$\Delta\nu_H = \frac{1}{2\pi} [(A_2 + k_2) + (A_1 + k_1) + 2\nu_{\text{col}}], \quad (3)$$

where A_j and k_j ($j=1,2$) are the rates of radiative emission and quenching rate of the upper and lower states, respectively, and ν_{col} is the total elastic collision frequency of the species. For the Xe($5p^56s$) and Xe($5p^56s'$) resonance

states the rates of radiative decay are 2.9×10^8 and $4.05 \times 10^8 \text{ s}^{-1}$, respectively.¹⁹ The reaction mechanisms and corresponding rate coefficients used to calculate the total quenching rates of these states are discussed in Ref. 11. Electron impact collisions (ionization, excitation to higher levels and de-excitation), which deplete the population of the resonance states, are the dominant quenching processes while the discharge is ignited and the electron density n_e and temperature T_e have large values ($n_e \approx 2 \times 10^{12} \text{ cm}^{-3}$, $T_e \approx 3\text{--}10 \text{ eV}$). The total elastic collision frequency for Xe with heavy particles was evaluated using

$$\nu_{\text{col}} = \sum_j \pi (\sigma_{\text{LJ}})^2 \nu_{\text{th}} N_j, \quad (4)$$

where σ_{LJ} is the first Lennard–Jones parameter, ν_{th} is the thermal speed of the Xe atoms, and the sum is performed over all collision partners j , having density N_j . For collisions between Xe and other gas species the average Lennard–Jones parameter is used.

In selecting the frequency of emission of photons, the Voigt line shape function was randomly sampled using an approach first described by Lee²⁰ which makes use of the concepts of joint and conditional probability density functions to avoid the use of numerical integration and look-up tables. After the ensemble is initialized, each pseudophoton is advanced along its trajectory until it is either reabsorbed by a ground state Xe atom or escapes from the discharge. Since both the ground state Xe density and temperature could vary due to gas heating or depletion, the mean free path for resonance absorption varies along the trajectory and so the null collision technique was employed.²¹ In this study, only gas phase reactions (electron impact and heavy particle collisions) and diffusion were considered in determining the ground state Xe density. Since the excitation fraction is typically $< 10^{-4}$, the ground state xenon concentration is essentially constant. The photon's trajectory is advanced over incremental steps, at each step checking whether the pseudophoton has (i) impinged on the phosphor or a non-transparent surface or (ii) exited the boundary of the computational mesh but is still within the physical system. If the photon hits an absorbing surface it is lost from the discharge and its properties are recorded. If the photon exits the mesh it is reinserted according to specified boundary conditions which, in this study, are periodic.

If the photon traverses its randomly selected trajectory without striking a surface, the type of absorption, real or ‘null’ is determined. In the case of a null absorption, a new mean free path is chosen and the photon is again advanced along its trajectory. If the photon is absorbed, the probability of re-emission, given by the ratio of the rate of spontaneous emission to the total quenching rate by radiative and nonradiative processes, is compared against another random number to determine whether the resulting excited state is quenched. If the random number is less than the re-emission probability the photon is relaunched with a new emission angle, and a new frequency randomly selected from the Voigt line shape. The mean free path for absorption is also

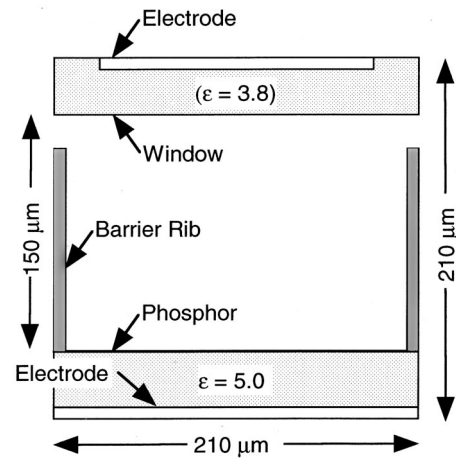


FIG. 1. Schematic of the opposing electrode PDP cell geometry. Voltage is applied to the top electrode. The bottom electrode is grounded. The barrier ribs are opaque to UV radiation.

recalculated and the earlier sequence is repeated until the excited state produced by the absorption is quenched or the photon escapes from the discharge.

III. PARTIAL TRAPPING AND LINE SHAPE

The MC–FR algorithm was implemented to investigate radiation transport, trapping and frequency redistribution in a PDP cell filled with a Ne/He/Xe = $(30-x)/70/x$ gas mixture at a pressure of 400 Torr ($x = 0.001\text{--}25$). The cell geometry for this study, shown in Fig. 1, has parallel plate electrodes, each separated from the gas by a layer of dielectric material, the lower of which is coated with phosphor. The width and height of the cell are $210 \mu\text{m}$, and the spacing between the dielectric layers is $150 \mu\text{m}$. The permittivities of the upper and lower dielectrics are $\epsilon = 3.8\epsilon_0$ and $\epsilon = 5\epsilon_0$, respectively, where ϵ_0 is the permittivity of free space. The opaque dielectric barrier ribs, $15 \mu\text{m}$ in thickness have a permittivity $\epsilon = 5\epsilon_0$. A single square-wave voltage pulse is applied to the upper electrode while the lower electrode is kept at ground potential. For each simulation the magnitude of the voltage pulse V_0 was adjusted to give a peak average electron density of approximately $2 \times 10^{12} \text{ cm}^{-3}$. For the range of xenon mole fractions studied here V_0 varies between 210 and 500 V.

A. Escape probabilities and emission spectra

Escape probabilities for 147 and 129 nm wavelength Xe photons are shown in Fig. 2 as a function of Xe mole fraction. The escape probability was obtained by invoking the MC–FR module at regular intervals and calculating the fraction of ‘pseudophotons’ that (i) escaped from the discharge (that is, were collected at any opaque surface) or (ii) were collected on the lower phosphor-coated dielectric surface. The escape probability is a measure of the likelihood that a single quanta of energy, which was originally transferred to a Xe atom by an inelastic collision with an electron or with another heavy particle and subsequently emitted as a photon, will leave the cell. To distinguish this quanta from photons which result from absorption and remission of other photons,

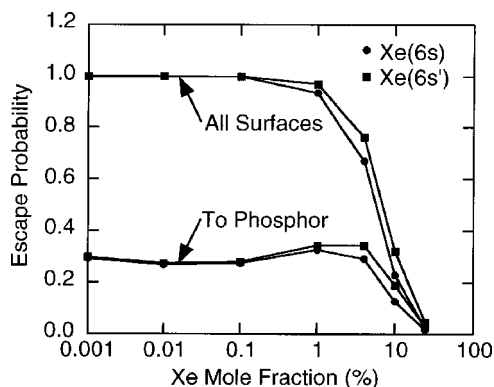


FIG. 2. Fraction of primary UV photons generated by the $\text{Xe}(5p^56s \rightarrow 5s^25p^6)$ and $\text{Xe}(5p^56s' \rightarrow 5s^25p^6)$ resonance transitions that (i) leave the discharge and (ii) reach the phosphor, for varying Xe mole fraction. As the Xe mole fraction increases, the radiation is trapped within the discharge for longer times, thereby allowing other quenching processes to compete with radiative emission resulting in a reduction in the escape probability.

the original quanta will be referred to as the *primary* photon. Due to an increase in electron impact quenching processes during the discharge, the escape probability generally varies over the duration of the voltage pulse, settling to a steady value after the discharge has been extinguished. The escape probabilities shown in Fig. 2 were averaged over 0.3–1.0 μs after the current pulse, a time when the majority of photons are emitted. The electron density and temperature continue to evolve during the postdischarge period and these effects are accounted for by solving the electron continuity and electron energy equations (as described in Ref. 11). Due to there being residual electric fields resulting from charging of the dielectrics, the electron temperature is 0.5–1 eV during this time.

At low concentrations of Xe (<0.1%) there are insufficient Xe atoms to produce appreciable quenching and trapping over the dimensions of the cell. The escape probability is therefore essentially unity and the radiation is in an optically thin regime. However, as the Xe mole fraction is increased to above 1%, photon trapping and quenching, which is dominated by collisions with other Xe atoms, both become significant causing the escape probability to fall. At 25% Xe concentration only a small fraction (<5%) of the primary photons ultimately leave the discharge. At these higher Xe concentrations the mean free path for resonance reabsorption is sufficiently short that collisional quenching processes begin to compete with radiative decay. Even though the total quenching rate is 2–3 orders of magnitude smaller than the vacuum radiative decay rate, the number of absorption-emission cycles is sufficiently large that most of the primary photons are eventually quenched and the radiation is in an optically thick regime. However, there exists a range of Xe mole fractions (1%–10%) for which the radiation is only in a partially thick regime. PDP cells are typically operated with Xe mole fractions that fall within this regime.

The probability that a photon will ultimately reach the phosphor, also shown in Fig. 2, does not change appreciably as the Xe concentration is increased from 0.001% to 0.1% and is about 30%. This low value results from the barrier ribs being opaque and intercepting radiation to the sides. The

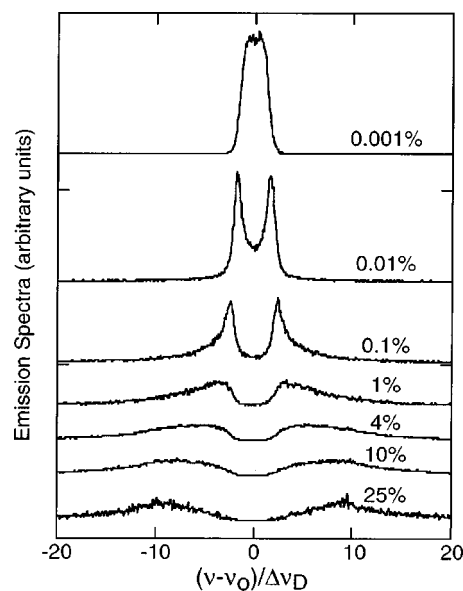


FIG. 3. Spectra of $\text{Xe}(5p^56s \rightarrow 5s^25p^6)$ photons incident on the phosphor for varying mole fractions of Xe. At low mole fractions, the radiation is not heavily trapped. At high mole fractions, significant trapping and collisions occur, resulting in redistribution of radiation to the wings of the transition.

fraction of photons reaching the phosphor exhibits a small maximum at Xe concentrations in the range 1%–4%, before falling to smaller values at higher concentrations of Xe. The cause of this behavior is related to the proximity of the source of resonance photons to the phosphor. At lower Xe concentrations (0.001%–0.1%) the $\text{Xe}(5p^56s)$ and $\text{Xe}(5p^56s')$ resonance state densities are concentrated in the region midway between the dielectric slabs, whereas at higher Xe concentration (1%–25%) the photon source regions are shifted toward the lower phosphor-coated dielectric. Therefore, despite the increase in radiation trapping and quenching at Xe concentrations of $\approx 1\%$, the trade-off is that the photons have a shorter distance to travel to reach the phosphor. There are many factors influencing this shift in the photon source region, among them being the lifetime of the discharge, the voltage required to sustain the discharge and the amount of surface charge accumulated on the dielectrics.

The spectra of 147 nm $\text{Xe}(5p^56s \rightarrow 5s^25p^6)$ photons that ultimately reached the phosphor are shown in Fig. 3 for various mole fractions of Xe. These spectra were collected and averaged over the steady postdischarge phase of the pulse (0.3–1.0 μs). (We confirmed that the spectra are essentially the same during the current pulse.) At low mole fractions of xenon the radiation is largely untrapped and the spectrum of radiation leaving the PDP cell is essentially the Voigt line shape, with a small depletion near line center. As the xenon concentration is increased, the mean free path for resonance absorption decreases and the effect of frequency redistribution on the line shape is increasingly more evident. The emission and absorption have higher probabilities of occurring near line center since that is where the oscillator strength is highest. There is, however, a small but finite probability that the photons will be re-emitted in the wings of the emission profile where the absorption cross section is smaller and the mean free path for reabsorption is longer. Even

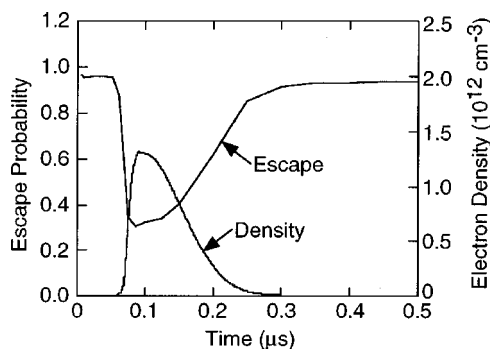


FIG. 4. Escape probability and spatially averaged electron density for a Xe mole fraction of 1%. Prior to the ignition of the discharge the escape probability for primary photons is at its maximum value. The increase in electron density and temperatures during the current pulse increases the electron impact quenching rates, causing a decrease in the escape probabilities. After the discharge is extinguished, however, the escape probabilities return to their initial values.

though a small fraction of the photons are, at any instant, emitted in the wings of the profile the fact that these photons have a longer mean free path results in them having a higher likelihood of escaping the plasma before being reabsorbed. As a result, as the xenon concentration increases, the observed emission spectrum becomes progressively depleted near line center and accentuated in the wings.

B. Effects of quenching processes on escape probabilities

The primary photon escape probability can vary considerably over the duration of the current pulse. Even though the mean free path for absorption remains essentially constant, while the discharge is ignited the electron density reaches sufficiently high values ($\approx 10^{12} \text{ cm}^{-3}$) that electron impact quenching processes start to compete with radiative decay and reabsorption. For example, the peak electron density for the $[\text{Xe}] = 1\%$ case is $3.9 \times 10^{12} \text{ cm}^{-3}$ at 100 ns. The electron temperature at that location about 2 eV. (The peak electron temperature is 4.2 eV.) Electron collision quenching for these conditions is dominated by $\text{Xe}(6s) \rightarrow \text{Xe}(6p)$ excitation with a total rate of $4 \times 10^6 \text{ s}^{-1}$. The consequences of electron collision quenching is demonstrated in Fig. 4 which shows the time dependence of the escape probability to any surface for primary $\text{Xe}(5p^56s)$ photons produced at the indicated times for $[\text{Xe}] = 1\%$. The volume-averaged electron density is also shown. The dip in the escape probability coincides with the maximum in electron density, a trend which occurs at all xenon mole fractions. (The effect is less severe at low xenon mole fractions and more severe at high xenon mole fractions.)

Note that the decrease in the escape probability does not imply a reduction in the total photon flux since the total magnitude of emission also increases. The primary quanta of energy being tracked which is quenched could also be recirculated back to the resonance state. For example, electron impact of $\text{Xe}(5p^56s)$ can produce an ion which, after dimerization, dissociatively recombines to produce another $\text{Xe}(5p^56s)$.

C. Transition from optically thin to optically thick transport

We have, for clarity, referred to primary photons as being *re-emitted* to describe the transport of the original quanta of energy through the discharge. However, each time a quantum of energy is *absorbed* by a ground state atom and *re-emitted* in the form of a photon all past information (for example, the site of last emission) is lost. The photons that reach the phosphor, are therefore, indistinguishable from the photons originally emitted and the only relevant information is the site of the last emission. By recording the site of last emission for each photon that reaches the phosphor, an effective source function for *untrapped* photons can be obtained. In an optically thick regime only photons emitted adjacent to the phosphor will reach it. In optically thin regimes, more extended sources are expected.

The source functions for untrapped $147 \text{ nm Xe}(5p^56s \rightarrow 5s^25p^6)$ photons for Xe mole fractions of 0.1%, 1%, and 4% are shown in Figs. 5–7, respectively. In order to highlight the role of frequency redistribution in the nonlocal nature of resonance photon transport, these source functions have been separated into three frequency bands: (a) less than three Doppler widths from line center, $|(\nu - \nu_0)/\Delta\nu_D| < 3$, (b) between three and ten Doppler widths from line center $3 < |(\nu - \nu_0)/\Delta\nu_D| < 10$, and (c) more than ten Doppler widths from line center, $|(\nu - \nu_0)/\Delta\nu_D| > 10$.

We first consider the case of $[\text{Xe}] = 0.1\%$ (Fig. 5) where photon trapping does not appreciably affect the average escape probability. The mean free path for absorption at line center $\lambda_a(\nu_0)$ is $\approx 0.4 \mu\text{m}$, which is ≈ 350 times smaller than the separation between the dielectrics. However, at 0.1% Xe the total quenching rate in the postdischarge phase of the discharge pulse is 4–5 orders of magnitude smaller than the radiative lifetime of the $\text{Xe}(5p^56s)$ state. Therefore, in the absence of frequency redistribution photons can undergo many emission-absorption cycles before having a significant chance of being quenched. As a result approximately 65% of the photons that reached the phosphor were emitted from distances further than $40 \mu\text{m}$ [$\approx 100\lambda_a(\nu_0)$] away. Of the photons that do reach the phosphor, those emitted at frequencies less than three Doppler widths from line center and thus having a shorter mean free path, are mostly likely to have been emitted in the immediate vicinity (within a few μm) of the phosphor. However, photons emitted with frequencies greater than three Doppler widths from line center are most likely to have originated from the center of cell where the $\text{Xe}(5p^56s)$ state density is a maximum.

As the mole fraction of Xe is increased to higher values (1% and 4%, shown in Figs. 6 and 7) the combined effects of radiation trapping and quenching become progressively more important. The source function for photons that reach the phosphor with frequencies near line center remains peaked within a few microns of the phosphor, as expected. However, due to the increase in the degree of frequency redistribution, a large fraction of the resonance photons incident on the phosphor were emitted further than $50 \mu\text{m}$ (approximately one third of the dielectric separation) from the phosphor. For example, at $[\text{Xe}] = 1\%$, 65% of the photons arrived from locations further than $20.5 \mu\text{m}$ [$\approx 500\lambda_a(\nu_0)$], while 38% ar-

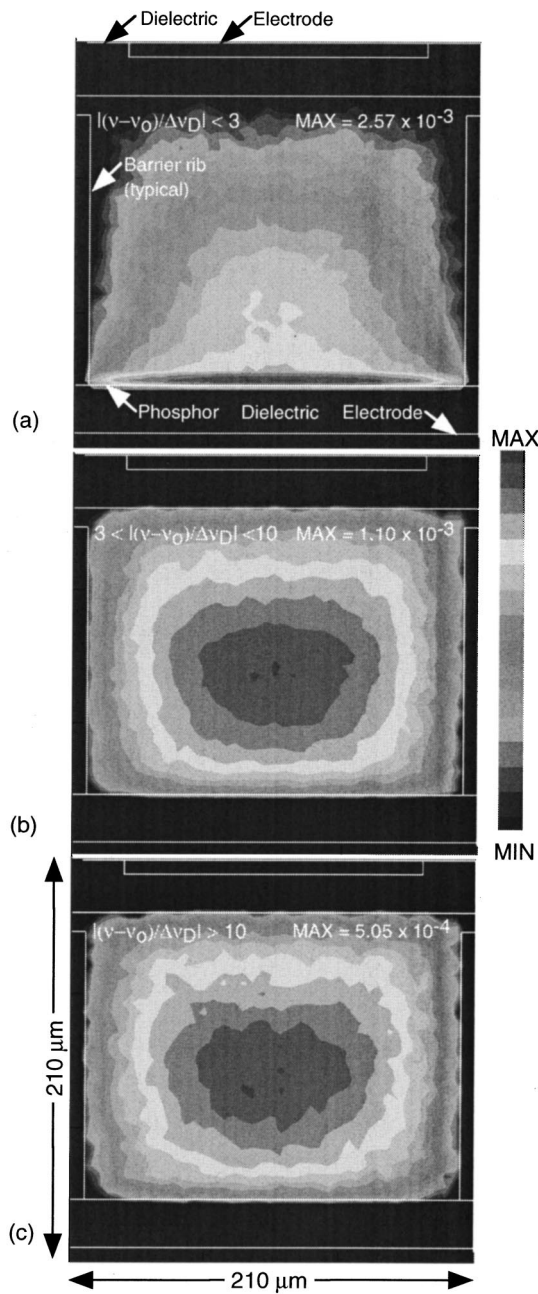


FIG. 5. Source functions for Xe($5p^5 6s \rightarrow 5s^2 5p^6$) photons that ultimately reach the phosphor for a xenon mole fraction $[Xe]=0.1\%$ in the frequency intervals: (a) $(\nu - \nu_0)/\Delta\nu_D < 3$, (b) $3 < (\nu - \nu_0)/\Delta\nu_D < 10$, and (c) $(\nu - \nu_0)/\Delta\nu_D > 10$. The plots use a log grayscale with a dynamic range of two decades. The maximum value for each case is indicated in the figure. Photons emitted with frequencies close to line center are optically thick and are therefore more likely to have been emitted in the vicinity of the phosphor. Photons emitted further out in the wings of the line shape can have a longer mean free path so the source function for the flux to the phosphor peaks where the total Xe($5p^5 6s$) density is highest, in the center of the cell.

rived from locations further than $41 \mu\text{m} [\approx 1000\lambda_a(\nu_0)]$. At $[Xe]=4\%$, 71% of the photons reaching the phosphor were emitted further than $10 \mu\text{m} \approx 1000\lambda_a(\nu_0)$ away, while 20% were emitted further than $50 \mu\text{m} [\approx 5000\lambda_a(\nu_0)]$ away.

Based on the results in Figs. 5–7, the assumption of optically thick resonance radiation (that is, that only photons emitted within a few mean free paths at line center of the

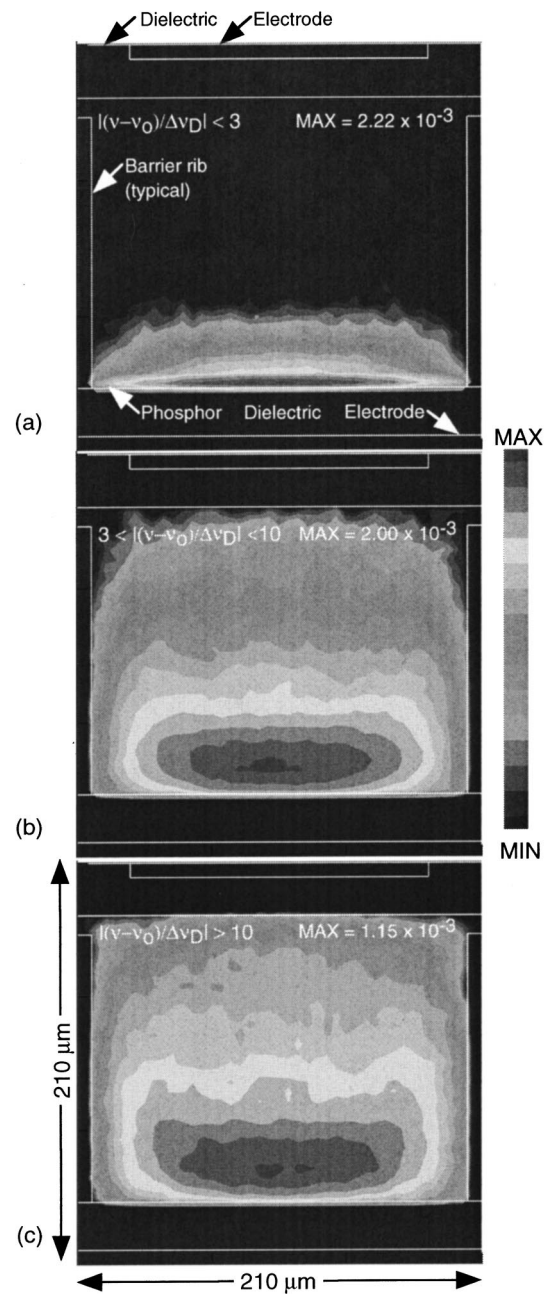


FIG. 6. Source functions for Xe($5p^5 6s \rightarrow 5s^2 5p^6$) photons that ultimately reach the phosphor for a xenon mole fraction of $[Xe]=1\%$ in the frequency intervals: (a) $(\nu - \nu_0)/\Delta\nu_D < 3$, (b) $3 < (\nu - \nu_0)/\Delta\nu_D < 10$, and (c) $(\nu - \nu_0)/\Delta\nu_D > 10$. The scaling of the plots is the same as in Fig. 5.

phosphor can reach it), is only valid for photons emitted with frequencies within a few Doppler widths of line center. For example, more than 80% of the photons incident on the phosphor were actually emitted from locations further than approximately 50, 250, and 500 absorption mean free paths (at line center) for xenon mole fractions of 0.1%, 1%, and 4%, respectively. The transition from optically thin to optically thick transport with increasing Xe mole fraction is demonstrated by Figs. 8 and 9. The fraction of Xe($5p^5 6s$) photons incident on the phosphor that were emitted further than a given distance from the phosphor is shown in Fig. 8. At low concentrations of xenon ($<4\%$) the radiation reach-

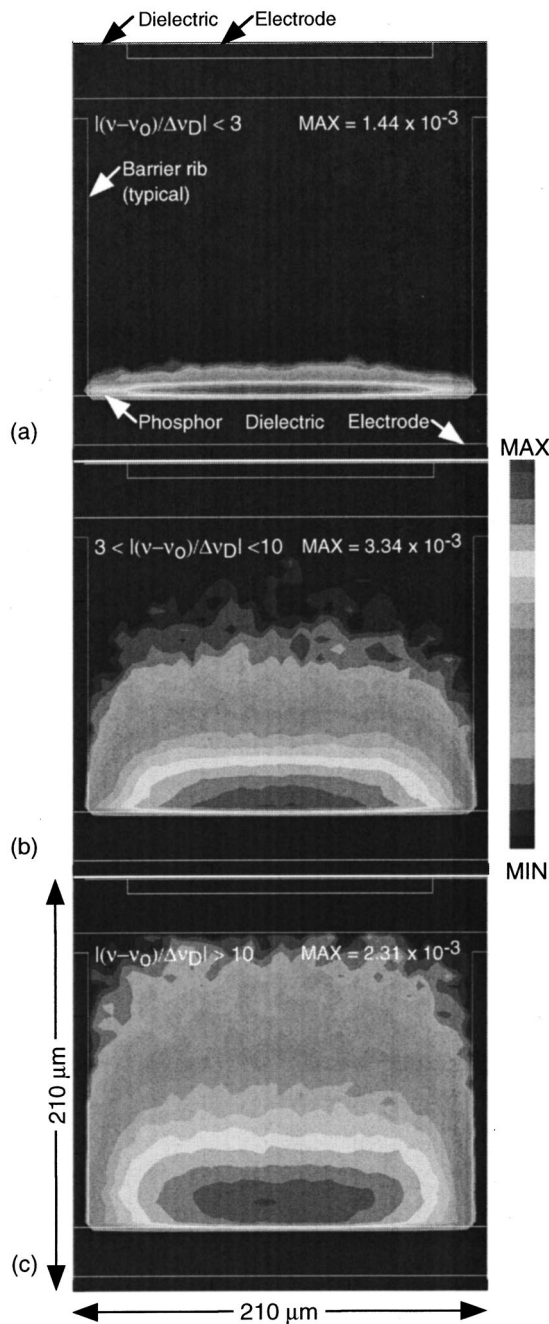


FIG. 7. Source functions for Xe($5p^5 6s \rightarrow 5s^2 5p^6$) photons that ultimately reach the phosphor for a xenon mole fraction of $[Xe]=4\%$ in the frequency intervals: (a) $|(v - \nu_0)/\Delta \nu_D| < 3$, (b) $3 < |(v - \nu_0)/\Delta \nu_D| < 10$, and (c) $|(v - \nu_0)/\Delta \nu_D| > 10$. The scaling of the plots is the same as in Fig. 5.

ing the phosphor is emitted from the entire volume of the cell and can therefore be described as optically thin. As the Xe concentration is increased, however, the fraction of these photons that are emitted remotely from the phosphor decreases, indicating a shift toward an optically thick regime. At $[Xe]=25\%$ roughly 75% of the photons were emitted within $15 \mu\text{m}$ of the phosphor. The relative contributions of Xe($5p^5 6s$) photons to the phosphor are shown in Fig. 9 for the three frequency bands: (a) $|(v - \nu_0)/\Delta \nu_D| < 3$, (b) $3 < |(v - \nu_0)/\Delta \nu_D| < 10$, and (c) $|(v - \nu_0)/\Delta \nu_D| > 10$. As the Xe concentration is increased the photons incident on the

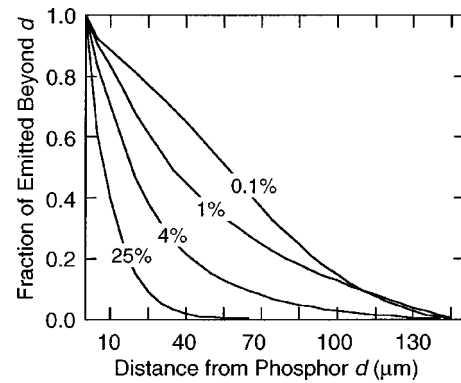


FIG. 8. Fraction of Xe($5p^5 6s \rightarrow 5s^2 5p^6$) photons incident on the phosphor that were emitted further than distance $d(\mu\text{m})$ from the phosphor, for various concentrations of Xe. At low Xe mole fractions, the source of resonance UV flux to the phosphor is distributed throughout the volume of the discharge. As the fraction of Xe in the gas mixture is increased the transition from optically thin to optically thick radiation transport is apparent.

phosphor are increasingly likely to have been emitted from the wings of the line shape. At $[Xe]=4\%$ more than half of the photons reaching the phosphor were emitted with frequencies more than ten Doppler widths from line center, with less than 5% emitted from the optically thick line center region.

IV. CONCLUDING REMARKS

Results from a model of resonance UV photon transport in a PDP cell, based on a MC-FR algorithm, have been presented. As the mole fraction of Xe is increased from 0.001% to 0.1% the fraction of primary photons that reach the phosphor remains at a relatively constant value of ≈ 0.3 . At these low concentrations of Xe radiation trapping and quenching are not important, as evidenced by the fact that more than half of the photons reaching the phosphor are emitted further than $\approx 35 \mu\text{m}$ away, and almost 100% of the photons eventually escaped the discharge. As the Xe concentration is increased to typical operating values ($\approx 4\%$), the fraction of primary photons that escape the discharge is re-

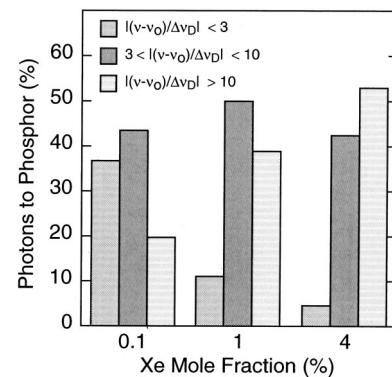


FIG. 9. Relative contributions of Xe($5p^5 6s \rightarrow 5s^2 5p^6$) photons incident on the phosphor from the three frequency bands: (a) $|(v - \nu_0)/\Delta \nu_D| < 3$, (b) $3 < |(v - \nu_0)/\Delta \nu_D| < 10$, and (c) $|(v - \nu_0)/\Delta \nu_D| > 10$. At low Xe mole fractions most of the resonance radiation reaching the phosphor is emitted from the core of the line shape. As the Xe concentration is increased radiation trapping becomes stronger and the emission is increasingly from the wings of the line shape.

duced, while the fraction that reach the phosphor remains essentially unchanged. This effect can be attributed to the shift in the resonance photon source region toward the lower dielectric at higher Xe concentrations. However, further increases in Xe mole fraction lead to a substantial reduction in both the fraction of photons that leave the discharge and the fraction that reach the phosphor. While the rate of production of resonance photons increases with Xe concentration, the absorption mean free path scales inversely with xenon concentration, increasing the degree of radiation trapping and subsequent quenching, and ultimately limiting the contribution of Xe resonance radiation to the production of visible light by the phosphor.

The results presented here also demonstrate that the assumptions of optically thick and optically thin radiation are not always appropriate for the conditions under which PDPs are typically operated. Even at Xe concentrations as high as 4%, where the effect of photon trapping and quenching start to become apparent, $\approx 30\%$ of the 147 nm Xe($5p^56s \rightarrow 5s^25p^6$) photon flux to the phosphor was emitted further than 35 μm from the phosphor. These photons were predominantly emitted from the wings of the line shape (more than 50% were emitted with frequencies further than ten Doppler widths from line center). The assumption of optically thick radiation will thus tend to underestimate the visible light output of the PDP cell. Likewise, the assumption of optically thin radiation transport is also likely not appropriate because $\approx 30\%$ of the 147 nm flux was emitted within 10 μm of the phosphor.

ACKNOWLEDGMENTS

This work was supported by LG Electronics Inc. The authors also wish to thank Shahid Rauf for useful discussions.

- ¹*Electronic Display Devices*, edited by S. Matsumoto (Wiley, New York, 1990).
- ²O. Sahni, C. Lanza, and K. Werner, *J. Appl. Phys.* **49**, 2365 (1978).
- ³O. Sahni and C. Lanza, *J. Appl. Phys.* **47**, 1337 (1976).
- ⁴O. Sahni and C. Lanza, *J. Appl. Phys.* **47**, 5107 (1976).
- ⁵R. Veerasingam, R. Campbell, and R. T. McGrath, *IEEE Trans. Plasma Sci.* **23**, 688 (1995).
- ⁶R. Campbell, R. Veerasingam, and R. T. McGrath, *IEEE Trans. Plasma Sci.* **23**, 698 (1995).
- ⁷P. J. Drallos, V. P. Nagorny, and W. Williamson, Jr., *Plasma Sources Sci. Technol.* **4**, 576 (1995).
- ⁸C. Punset, J. P. Boeuf, and L. C. Pitchford, *J. Appl. Phys.* **83**, 1984 (1998).
- ⁹J. Meunier, Ph. Belenguer, and J. P. Boeuf, *J. Appl. Phys.* **78**, 731 (1995).
- ¹⁰R. Veerasingam, R. B. Campbell, and R. T. McGrath, *Plasma Sources Sci. Technol.* **6**, 157 (1997).
- ¹¹S. Rauf and M. J. Kushner, *J. Appl. Phys.* **85**, 3460 (1999).
- ¹²S. Rauf and M. J. Kushner, *J. Appl. Phys.* **85**, 3470 (1999).
- ¹³T. Holstein, *Phys. Rev.* **72**, 1212 (1947); **83**, 1159 (1951).
- ¹⁴J. J. Curry, J. E. Lawler, and G. G. Lister, *J. Appl. Phys.* **86**, 731 (1999).
- ¹⁵J. E. Lawler and J. J. Curry, *J. Phys. D: Appl. Phys.* **31**, 3235 (1998).
- ¹⁶H. M. Anderson, S. D. Bergeson, D. A. Doughty, and J. E. Lawler, *Phys. Rev. A* **51**, 211 (1995).
- ¹⁷R. R. Meier and J.-S. Lee, *Planet. Space Sci.* **30**, 439 (1982).
- ¹⁸J. T. Verdeyen, *Laser Electronics* (Prentice-Hall, Englewood Cliffs, NJ, 1989), p. 71.
- ¹⁹M. Aymar and M. Coulombe, *At. Data Nucl. Data Tables* **21**, 537 (1978).
- ²⁰J.-S. Lee, *Astrophys. J.* **197**, 159 (1974); **192**, 465 (1974).
- ²¹H. R. Skullerud, *J. Phys. D* **1**, 1567 (1968).